Volume 11
Number 25
7 July 2023
Pages 5621–5924

Journal of Materials Chemistry B

Materials for biology and medicine

rsc.li/materials-b

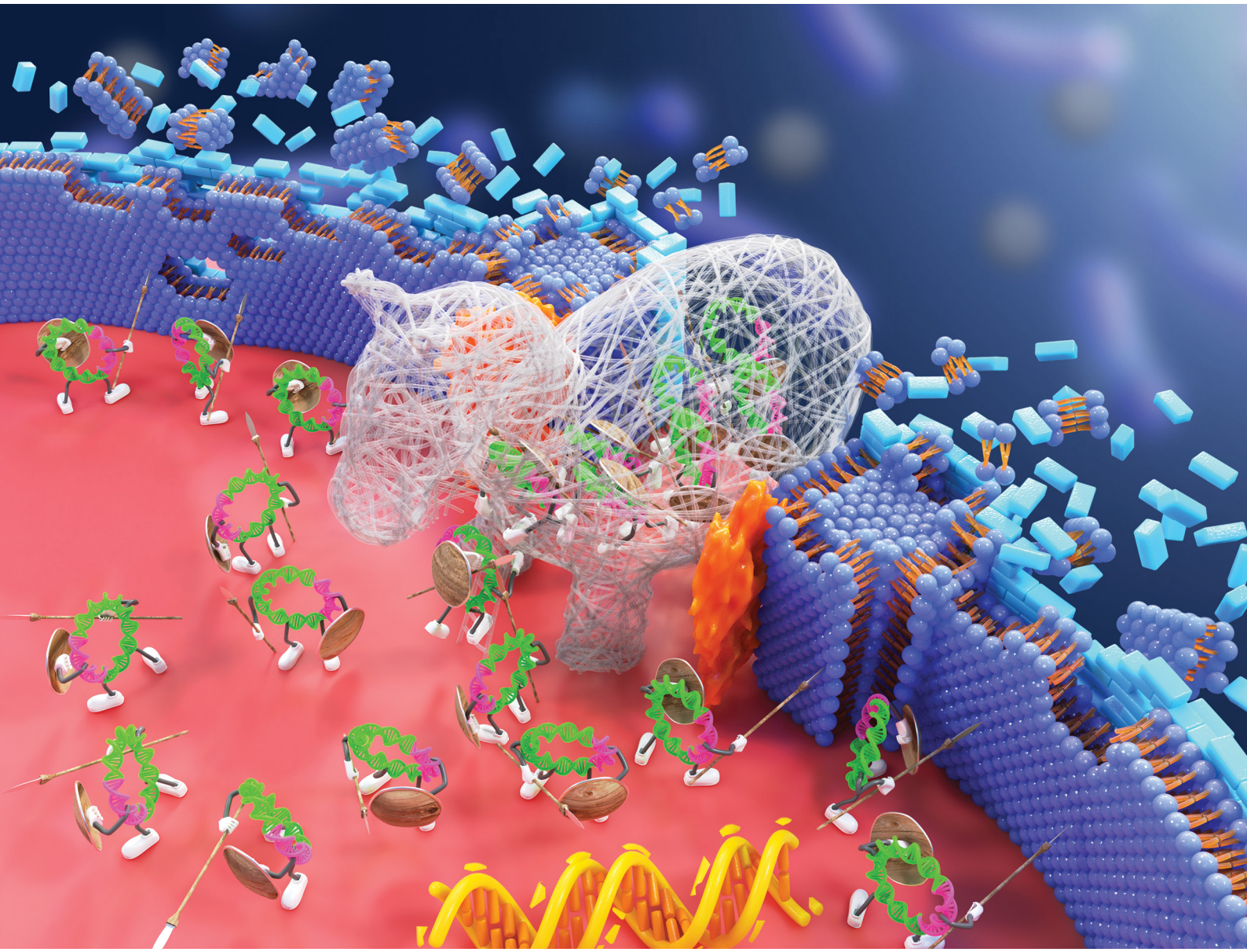

ISSN 2050-750X

ROYAL SOCIETY OF CHEMISTRY

PAPER

Yingming Yang, Tao Hu *et al.*
Spermine-starch nanoparticles with antisense *vicR* suppress *Streptococcus mutans* cariogenicity

10 YEARS ANNIVERSARY

Journal of Materials Chemistry B

ROYAL SOCIETY OF CHEMISTRY

PAPER

View Article Online
View Journal | View Issue

Cite this: J. Mater. Chem. B, 2023, 11, 5752

Spermine-starch nanoparticles with antisense *vicR* suppress *Streptococcus mutans* cariogenicity†

Lei Lei,‡[a] Yue Zhang,‡[a] Yichen Xu,‡[b] Yuting Tian,[a] Jialiang Zhao,[a] Yong Xiang,[a] Huiyu Yang,[a] Yingming Yang*[a] and Tao Hu *[a]

Dental caries of permanent teeth is a common public health concern and has the second-highest incidence among global diseases. The exopolysaccharides (EPS) synthesized by *Streptococcus mutans* (*S. mutans*) are the principal virulence factor for cariogenic etiology. We previously discovered that an endogenous antisense *vicR* RNA (AS*vicR*) could significantly inhibit EPS synthesis in *S. mutans* and reduce its cariogenicity. However, AS*vicR* cannot be directly applied in the oral environment. An appropriate vector is of great need to protect AS*vicR* from being degraded by nucleases for effective gene delivery to *S. mutans*. Functionally modified starches shed light on this field because of their excellent biocompatibility and biodegradability. In this study, a biocompatible and biodegradable spermine-starch nanocomposite (SSN) was constructed for AS*vicR* delivery. Starch was cationically functionalized by grafting endogenous spermine to closely bind with the recombinant AS*vicR* plasmid. The SSN not only protected the recombinant AS*vicR* plasmid from DNase I but also achieved highly efficient gene transformation to *S. mutans via* the hydrolysis of α-amylase in the saliva. In addition, SSN-AS*vicR* was shown to endow AS*vicR* with an increasing transformation efficiency approximately four times that of the naked AS*vicR* plasmid, as well as allowing for targeting specificity to the transcription of the *vicR* gene and the suppression of biofilm organization *via* EPS digestion. In particular, SSN-AS*vicR* nanoparticles exhibited excellent biological safety and maintained oral microbiota homeostasis *in vivo*. The SSN can be prepared in a ready-to-use formulation for targeting cariogenic bacteria, thus demonstrating important prospects in the prevention of dental caries.

Received 1st December 2022,
Accepted 3rd April 2023

DOI: 10.1039/d2tb02628g

rsc.li/materials-b

1. Introduction

As one of the most prevalent oral diseases, dental caries threatens the well-being of every individual. The incidence of permanent tooth caries was the second-highest among global diseases affecting the world's population.[1] Etiologically, dental caries is an infectious disease on the tooth surface. *Streptococcus mutans* (*S. mutans*) is the principal decay-causing bacterium due to its capability to synthesize exopolysaccharides (EPS) that can further form a cariogenic biofilm on the tooth surface.[2] The *S. mutans* VicRK two component signal transduction system (TCS) regulates genes that are associated with EPS synthesis, genetic competence, oxidative stress response, and cell wall homeostasis, and they are conserved in other Gram-positive coccus species.[3,4] In particular, these EPS synthesis-associated genes, including *gtfB/C* and *gbpB*, are positively regulated by VicR. Moreover, *vicR* deletion mutants have been unable to be constructed, thus suggesting that *VicR* is essential for viability and controls the expression of virulence genes.[5] Notably, in our previous studies, we identified an endogenous antisense *vicR* RNA (AS*vicR*) and verified that the overexpression of AS*vicR* could inhibit the transcription and translation of the *vicR* gene.[6,7] *Via* RNA interference (RNAi), AS*vicR* can downregulate the expression of glucosyltransferases (GtfB, GtfC, and GtfD), thus significantly inhibiting EPS synthesis and reducing the cariogenicity of *S. mutans*.[7] On the other hand, dextranase A (DexA) participates in the degradation of exopolysaccharides by hydrolyzing glycosidic bonds.[8,9] Nevertheless, ubiquitous deoxyribonucleases (DNases) can severely limit the application of AS*vicR* in the oral environment. Therefore, an appropriate vector is urgently needed for efficient AS*vicR* delivery.

Although various materials (such as viral vectors, lipid-based particles, and polymeric particles) have been explored as protective nucleic acid carriers, the biocompatibility and safety of

[a] State Key Laboratory of Oral Diseases, Department of Preventive Dentistry, West China Hospital of Stomatology, Sichuan University, 14# Third Section Renmin South Road, Chengdu, 610041, China. E-mail: ymyang@scu.edu.cn, hutao@scu.edu.cn

[b] State Key Laboratory of Oral Diseases, Department of Oral Prosthodontics, West China Hospital of Stomatology, Sichuan University, 14# Third Section Renmin South Road, Chengdu, 610041, China

† Electronic supplementary information (ESI) available. See DOI: https://doi.org/10.1039/d2tb02628g

‡ These authors contributed equally to this work.

these vectors remain controversial.[10,11] For Gram-positive cocci, a cell-penetrating peptide agent was used to facilitate oligonucleotide transformation, but their inherent toxicity and poor stability have restricted their applications.[12] Recent progress in materials science has indicated that naturally obtainable starch is promising for biomedical applications, such as blood-absorbing collagen sponges,[13] nano-encapsulating agents,[14] and drug delivery systems.[15] As a gene vector applied to the oral cavity, starch may possess superior biocompatibility and biodegradability[16] compared to virus-based and artificially synthesized vectors. The starch vector can also be hydrolyzed by amylase in saliva, thus achieving gene delivery in an innovative manner. In our recently published work,[17] we constructed the aminated dendritic mesoporous silica nanoparticles (DMSNs-NH_2) carrying plasmid-AS*vicR*. However, the use of DMSNs-NH_2 is restricted by its non-degradable properties.

Attempts have previously been made to modify starch molecules with positively charged quaternary ammonium groups.[18] However, toxicological reports of quaternary ammonium compounds have raised significant concerns regarding their harmful effects on human health, such as oxidative stress, DNA damage, mitochondrial apoptosis, and cell death.[19,20] For biomedical applications, spermine is a biofriendly and endogenous tetraamine with two primary and two secondary amino groups. Madeo *et al.* reported that dietary supplementation with polyamines is a protective strategy to increase longevity.[21] In addition, polyamines have been shown to promote mitochondrial respiration and delay brain aging.[22] The positive charge of spermine under physiological conditions allows it to bind and stabilize nucleic acids, which provides favorable conditions for DNA transport.

In this study, we utilized starch and spermine to construct a gene vector for AS*vicR* plasmid delivery. The starch molecule was cationically functionalized by grafting the spermine molecule *via* 1,1′-carbonyldiimidazole (CDI) activation. The spermine-starch nanocomposite (SSN) was capable of loading AS*vicR* *via* electrostatic interactions. The SSN was effective in protecting AS*vicR* from nuclease degradation, thus achieving highly efficient gene transformation to *S. mutans*. After treatment with SSN-AS*vicR* by mouth rinsing, the EPS synthesis of *S. mutans* was inhibited. An *in vivo* animal study further demonstrated the impediment effect of SSN-AS*vicR* on dental caries. Innovatively, this biocompatible and biodegradable SSN material shows important prospects in the prevention of dental caries. More importantly, the vector construction strategy may provide a novel approach for targeted nonantibiotic treatment against bacterial infection.

2. Materials and methods

2.1 Materials

Pullulanase, anhydrous dimethylsulfoxide (DMSO), CDI, and chemically pure grade PEG20000 were purchased from Macklin Reagent Company (Shanghai, China). α-Amylase, spermine, dialysis bags (7000D), cornstarch, DNase I, and the calcein-AM/PI kit were commercially obtained from Solaibio Reagent Company (Beijing, China). Agarose, brain heart infusion, and Dulbecco's modified Eagle medium (DMEM) were bought from Thermo Fisher Scientific (MA, USA). Additionally, the EndoFree Plasmid Kit (Tiangen, Beijing, China), the MasterPure RNA purification Kit (Epicentre, MD, USA), the RevertAid First Strand cDNA Synthesis Kit (Thermo Fisher Scientific), and the Cell Counting Kit-8 (CCK-8, Dojindo, Japan) were used in the present study.

2.2 Sample preparation

2.2.1 Preparation of degraded starch. 5% starch was gelatinized at 80 °C for 30 minutes and then cooled at room temperature until it reached 60 °C. Pullulanase was added to hydrolyze the gelatinized starch for 12 h, and then the solution was heated at 95 °C for 30 minutes to inactivate pullulanase. After the temperature of the solution reached 60 °C by incubating at room temperature, α-amylase was added to hydrolyze the gelatinized starch for 1 h, and the solution was heated to 95 °C for 30 minutes to inactivate α-amylase. After cooling to room temperature, the precipitant was concentrated by centrifugation. The solution was dialyzed against pure water (molecular weight cutoff of 7000 Da) for 24 h and then lyophilized. The composition flowchart of spermine modified starch-AS*vicR* nanoparticles is shown in ESI† Fig. S1.

2.2.2 Preparation of a spermine-starch nanocomposite (SSN). Spermine was introduced into the hydroxyl groups of starch using the CDI activator.[23] Specifically, starch (20 mg mL^{-1} in anhydrous DMSO) was activated by CDI. CDI was mixed with the glucose units of starch at molar ratios of 1 : 2, 1 : 4, and 1 : 6 for 2 h at room temperature. Then, spermine (CDI : spermine molar ratio of 1 : 1) was added and the reactions were continued at 35 °C for 24 h. When the reactions were complete, the products were dialyzed against pure water (molecular weight cutoff of 7000) for three days and lyophilized. The obtained samples were named SSN-1, SSN-2, and SSN-3.

2.2.3 Preparation of SSN-ASvicR. PDL278 plasmids containing AS*vicR*[7] or AS*vicR-gfp* sequences were acquired from recombinant *E. coli* using the EndoFree Plasmid Kit, and the NanoDrop One (Thermo Fisher Scientific) was used to determine the plasmid concentrations. SSN-1 was mixed with deionized water in a capped tube to prepare the SSN (50 mg μL^{-1}). The solution was heated at 40 °C using a temperature-controlled water bath for 15 min to totally dissolve SSN-1. The plasmid solution was finally mixed with the SSN-1 solution at a mass ratio of 1 : 8 to prepare the dispersed phase. Polyethylene glycol (PEG) was dissolved in deionized water to produce a PEG solution with a final concentration of 33.1 g/100 mL. The PEG solution (continuous phase) was agitated at 500 rpm in a water bath at 70 °C for 1 h. When the temperature of this continuous phase dropped to 40 °C, the solution was transferred to centrifuge tubes, and then the dispersed phase was gently poured into the continuous phase (v/v = 1 : 8).

A vortex oscillator was used to vibrate the solution for 10 min. The obtained emulsion was refrigerated at 4 °C for 24 h to solidify the droplets. Finally, the prepared emulsion was centrifuged at 5000 rpm for 15 min. The sediment (SSN-AS*vicR* nanoparticles)

was washed twice with 75% ethanol, dehydrated with absolute ethanol, and dried in an oven at 50 °C for 24 h. The dried microspheres were sealed and stored in a desiccator for further investigations.[23]

2.3 Materials characterization

2.3.1 Molecular weight analysis. The weight average molecular weight (M_w) and molecular weight distribution for degraded starch were determined by gel permeation chromatography (GPC) (Waters China Ltd). The samples were prepared at a concentration of 5 mg mL^{-1} in a filtered mobile phase (0.1 M $NaNO_3$ solution with 0.02% w/v NaN_3, which had been filtered through a 0.22 μm cellulose nitrate filter). The flow rate and column temperature of the GPC system were set at 0.6 mL min^{-1} and 35 °C, respectively.

2.3.2 Fourier transform infrared spectroscopy test. Fourier transform infrared (FTIR) spectroscopy analysis was performed using a Tensor 37 spectrophotometer (Bruker Instrument Co., Germany). 32 scans per spectrum were acquired from degraded starch, SSN-1, SSN-2, and SSN-3 samples in the 4000–400 nm cm^{-1} range with a resolution of 4 cm^{-1}.

2.3.3 ^{1}H nuclear magnetic resonance evaluation. A ^{1}H nuclear magnetic resonance (^{1}H NMR) test was performed to analyze degraded starch, SSN-1, SSN-2, and SSN-3 dissolved in D_2O using an NMR spectrometer (AVANCE 400, Bruker, Germany). Chemical shifts were referenced to the solvent peak, δ = 4.70 ppm. Data were processed by MestReNova software (12.0.2, Mestrelab Research S. L., Spain).

2.3.4 Zeta potential measurement. For zeta potential measurements, AS*vicR*, SSN-1, SSN-2, SSN-3, and SSN-AS*vicR* solution samples (n = 7) were dropped on the coverslip and measured using a Zetasizer (Nano ZS; Malvern Instruments, Malvern, UK).

2.3.5 Elemental analysis. The nitrogen contents of SSN-1, SSN-2, and SSN-3 (n = 4) were measured by elemental analysis (EA) using a CHNS elemental analyzer (Vario EL cube, Elementar, Germany). Briefly, the samples were statically burned in pure oxygen at 1800 °C to obtain a gas mixture composed of CO_2, H_2O, N_2, and nitrogen oxides. Next, in a reduction tube, excess oxygen was removed, and nitrogen oxides were reduced to N_2. The gas mixture was then separated using a gas chromatographic column and analyzed using a thermal conductivity detector. The obtained mass percentage of nitrogen (N%) was used to further characterize the amount of spermine grafted onto the degraded starch. The molar ratios of spermine to glucose unit of starch (R) in SSN-1, SSN-2, and SSN-3 were determined using eqn (1):

$$R = \frac{162\ \mathrm{N}\%}{56 - 216\ \mathrm{N}\%} \quad (1)$$

The grafting efficiency (E) of spermine was obtained from eqn (2):

$$E = \frac{R}{R_0} \times 100 \quad (2)$$

where R_0 is the molar ratio of spermine to glucose unit of starch before reaction. As described in Section 2.2.2, R_0 of SSN-1, SSN-2, and SSN-3 is 1 : 2, 1 : 4, and 1 : 6, respectively. The weight percent (wt%) of spermine in SSN-1, SSN-2, and SSN-3 was calculated using eqn (3):

$$\mathrm{wt}\% = \frac{201\ \mathrm{N}\%}{56} \times 100 \quad (3)$$

2.3.6 Scanning electron microscopy (SEM) analysis. To investigate the morphology and particle size in different dispersion liquids, the SSN-AS*vicR* nanoparticles were dispersed in deionized water and ethanol, respectively. The two suspensions were smeared onto glass slides and subsequently dried in air at room temperature for 6 h. Afterwards, the specimens were sputter-coated with gold (Au) for 30 seconds and observed using a high vacuum FEG source scanning electron microscope (Inspect F, FEI Company, Hillsboro, OR, USA). Representative images were taken at 80 000× and 160 000× magnifications at an accelerating voltage of 20 kV.

2.3.7 Agarose gel electrophoresis. SSN-1, SSN-2, and SSN-3 were mixed with AS*vicR* plasmid at mass ratios of 2 : 1, 4 : 1, and 8 : 1 for 30 min to investigate the binding ability of the materials. The SSN-AS*vicR* nanoparticles are mixed with α-amylase or/and DNase at 60 °C in a water bath for 15 min. Next, the mixtures were analyzed by 1% agarose gel electrophoresis in tris-acetate (TAE) buffer at 100 V for 30 min. The resulting DNA products were observed under UV irradiation using a Bio-Rad electrophoresis system (Bio-Rad Laboratories, CA, USA).

2.4 Bacterial biofilm experiments

2.4.1 Bacterial growth. The *S. mutans* UA159 strain was provided by the State Key Laboratory of Oral Diseases (Sichuan University, Chengdu, China). *S. mutans* strains were routinely grown in Brain Heart Infusion (BHI) media at 37 °C anaerobically (90% N_2, 5% CO_2, and 5% H_2) as described previously.[24] *S. mutans* cells were cultured to the mid-exponential phase (cell optical density at 600 nm [OD_{600}] 0.5) in BHI medium and a total of 50 μL of mid-log-phase cells was inoculated into 1 mL BHI medium.

2.4.2 Bacterial transformation evaluation. Recombinant AS*vicR* plasmids were labeled with a gene encoding enhanced green fluorescent protein (AS*vicR-gfp*). The shuttle vector pDL278 was used to construct and express the AS*vicR-gfp* sequences (listed in the ESI†) under the control of the *S. mutans* promoter region of *vicR*. First, the antisense AS*vicR-gfp* sequences were obtained by oligonucleotide synthesis (Sangon Biotech, Shanghai, China), and, in addition, the promoter sequence of *vicR* was synthesized. Next, the sequences were cloned into vector pDL278 at BamHI and EcoRI restriction sites, generating recombinant plasmid pDL278AS*vicR-gfp*. *S. mutans* UA159 cultures were grown before the mid-exponential phase ($OD_{600\,nm}$ = 0.2).[25,26] For the transformation of the naked AS*vicR-gfp* plasmid without the competence stimulating peptide (CSP), two hundred nanograms of recombinant AS*vicR-gfp* were added to 500 μL of *S. mutans* culture ($OD_{600\,nm}$ = 0.2) and incubated for 2 h at 37 °C anaerobically (90% N_2, 5% CO_2, and 5% H_2). For the transformation of the naked AS*vicR-gfp* plasmid with the competence stimulating peptide (CSP), CSP was added to 500 μL of *S. mutans* culture ($OD_{600\,nm}$ = 0.2) to achieve a final concentration of 1 μg mL^{-1}. Two hundred nanograms of recombinant AS*vicR-gfp* were added to the culture and incubated for 2 h at 37 °C anaerobically

(90% N_2, 5% CO_2, and 5% H_2). For the transformation of SSN-AS*vicR-gfp*, 1.8 micrograms of SSN-AS*vicR-gfp*, which contained 200 ng AS*vicR-gfp*, were added to 500 μL of *S. mutans* culture ($OD_{600\,nm}$ = 0.2) and incubated for 2 h. For the transformation of SSN (the nanoparticle vector minus plasmid), 1.6 micrograms of SSN and 200 ng recombinant AS*vicR-gfp* were added to 500 μL of *S. mutans* culture ($OD_{600\,nm}$ = 0.2) and incubated for 2 h. Untreated *S. mutans* was set as blank control.

After SSN-AS*vicR-gfp*, AS*vicR-gfp* with CSP, AS*vicR-gfp* without CSP or SSN plus AS*vicR-gfp* treatment, 50 μL bacterial suspensions (n = 5) were dropped on coverslips and dried in air at room temperature for 30 minutes. Then, the planktonic bacterial cells were stained with 5 μg mL^{-1} Alexa-555 WGA (Invitrogen) for 10 minutes in the dark. Confocal laser scanning microscopy (CLSM) was applied to observe the expression level of eGFP. The transformation of AS*vicR-gfp* was qualitatively assessed by observing green fluorescence intensities. The quantification of AS*vicR-gfp* transformation has been compared with the expressions of *gfp* genes by quantitative real-time PCR described in 4.5.

After SSN-AS*vicR-gfp*, AS*vicR-gfp* with CSP, AS*vicR-gfp* without CSP or SSN plus AS*vicR-gfp* treatment, the selective plating cell counting assay was conducted. One hundred microliters of bacterial suspensions were coated on BHI plates containing 1000 μg mL^{-1} spectinomycin for selection and incubated for 48 h at 37 °C anaerobically (90% N_2, 5% CO_2, and 5% H_2). For the flow cytometry assays, 500 μL bacterial suspensions were collected after SSN-AS*vicR-gfp*, AS*vicR-gfp* with CSP, AS*vicR-gfp* without CSP or SSN plus AS*vicR-gfp* treatment. Untreated *S. mutans* was set as background control. The average fluorescence intensity of GFP was detected immediately, analyzed using a flow cytometer (Beckman Coulter, USA) and the fluorescence above the background level was calculated.[27]

2.4.3 Biofilm structural formation for SEM analysis. Overnight *S. mutans* cultures were grown to the mid-exponential phase in BHI medium. The suspension of *S. mutans* UA159 was followed by diluting 100 μL culture into 2 mL of fresh BHI supplemented with 1% (w/v) sucrose at 37 °C anaerobically (90% N_2, 5% CO_2, and 5% H_2).[6,7] The biofilms were established on the glass plates in 12-well plates. To determine the optimum concentrations of SSN-AS*vicR*, 3.6 μg, 14.4 μg, and 28.8 μg of SSN-AS*vicR* were added to the culture in each well respectively every 4 h during 12 h incubation. Then, the biofilms were formed in the presence of SSN-AS*vicR* from 12 h to 24 h incubation at 37 °C anaerobically (90% N_2, 5% CO_2, and 5% H_2). To investigate the regulatory effects of SSN-AS*vicR* on biofilm formation *in vitro*, 24-h bacterial biofilm experiments were analyzed by SEM as previously described.[7] Briefly, *S. mutans* biofilms on glass plates were washed twice with PBS and fixed with 2.5% glutaraldehyde at room temperature for 4 h. Serial dehydration included preparations with ethanol solutions (30%, 50%, 70%, 95%, and 100%), critical-point drying with liquid CO_2, and coating with gold powder. Biofilm specimen scanning electron micrographs were obtained with a scanning electron microscope (Inspect Hillsboro, OR, USA). Three biological replicated samples were included and each sample was technically replicated three times.

2.4.4 Biofilm EPS production and CLSM analysis. To further investigate the effects of SSN-AS*vicR* on biofilm EPS production, overnight *S. mutans* cultures were grown to the mid-exponential phase in BHI medium. The suspension of *S. mutans* UA159 was followed by diluting 100 μL culture into 2 mL of fresh BHI supplemented with 1% (w/v) sucrose according to our previous studies[6,7] at 37 °C anaerobically (90% N_2, 5% CO_2, and 5% H_2). The biofilms were established on the glass plates in 12 well plates. For SSN-AS*vicR* treatment, 28.8 μg of SSN-AS*vicR* were added to the culture in each well every 4 h during 12 h incubation and the biofilms were formed in the presence of SSN-AS*vicR* from 12 h to 24 h incubation at 37 °C anaerobically (90% N_2, 5% CO_2, and 5% H_2). For AS*vicR* treatment, 3.2 μg of AS*vicR* plasmid were added to the culture in each well every 4 h during 12 h incubation and the biofilms were formed in the presence of AS*vicR* from 12 h to 24 h incubation at 37 °C anaerobically. For SSN treatment, 25.6 μg of SSN were added to the culture in each well every 4 h during 12 h incubation and the biofilms were formed in the presence of the SSN from 12 h to 24 h incubation at 37 °C anaerobically. Untreated *S. mutans* was set as blank control. The biofilm EPS production after treatment was analyzed by CLSM as previously described.[7] The EPS matrix of *S. mutans* biofilms was stained with the Alexa 647-labeled dextran conjugate (Invitrogen, Eugene, OR, USA), and bacterial cells in the biofilm were labeled with SYTO9 (Invitrogen, Carlsbad, CA, USA). Next, confocal laser scanning microscopy was performed using a microscope (CLSM, TSP SP2; Leica, Solms, Germany) at 63× magnification using an oil-immersion objective lens. Three-dimensional reconstruction of the biofilms as well as imaging of biomass quantification was analyzed using Imaris 7.0 software (Bitplane, Zurich, Switzerland). Calculations of cell biomass reported, EPS biomass, and biofilm thickness were performed with COMSTAT as previously described.[28] Three biological replicated samples were included. Experiments were performed in triplicate for three randomly selected areas of each specimen.

2.4.5 Transcription analysis. The biofilm samples of *S. mutans* treated with SSN, AS*vicR* and SSN-ASvicR respectively were prepared as described in 4.4. For planktonic cultures, overnight *S. mutans* cultures were grown to the mid-exponential phase in BHI medium. The suspension of *S. mutans* UA159 was followed by diluting 100 μL culture into 2 mL of fresh BHI. For SSN-AS*vicR* treatment, 28.8 μg of SSN-AS*vicR* were added to the culture and incubated for 3 h. For AS*vicR* treatment, 3.2 μg of AS*vicR* plasmid were added to the culture and incubated for 3 h. For SSN treatment, 25.6 μg of SSN were added to the culture and incubated for 3 h. Untreated *S. mutans* was set as blank control.

Total RNAs of *S. mutans* in biofilm or planktonic cultures were extracted using a MasterPure RNA purification Kit (Epicentre, MD, USA). After biofilms were established for 24 h, the biofilm samples were harvested by scraping using a cell scraper and resuspended in PBS buffer. The bacterial cells were collected by centrifugation (4500 rpm, 4 °C) for 15 min and then resuspended in tissue and cell lysis solution (MasterPure

RNA purification Kit). The planktonic cells were collected by centrifugation (4500 rpm, 4 °C) for 15 min, washed with PBS buffer and resuspended in tissue and cell lysis solution (MasterPure RNA purification Kit). The genomic DNA was removed by digestion with Turbo RNase-free DNase I (Ambion, Austin, TX, USA) according to the manufacturer's instructions. The purity (A260/A280) and concentration of RNA were determined using a NanoDrop2000 spectrophotometer (Thermo Scientific, Waltham, MA, USA). RNA samples were reverse transcribed to complementary DNA (cDNA) using random 6 mers or gene-specific primer for AS*vicR* (Table S1, ESI†) with the RevertAid First Strand cDNA Synthesis Kit (Thermo Scientific, MA, USA). Real-time PCR was carried out with a Bio-Rad Applied Biosystems ABI 7500 System (Bio-Rad Laboratories, Hercules, CA, USA). For each real-time PCR reaction, 20 μL of a mixture containing 10 μL SYBR Premix Ex TaqII, 2.0 μL template cDNA, 1 μL 10 μM PCR Forward Primer, 1 μL 10 μM PCR Reverse Primer, 0.4 μL ROX Reference Dye, and 5.6 μL deionized water was placed in each well. Primers used in real-time PCR reactions are shown in ESI,† Table S1 and were obtained commercially (Sangon Biotech, Shanghai, China). Conditions for real-time PCR were as follows: 95 °C, 3 min (initial denaturation), followed by 35 cycles at 95 °C for 30 s (denaturation), 55 °C for 30 s (primer annealing), and 72 °C for 30 s (extension). Threshold cycle values (CT) were quantified and the expression of each gene was normalized relative to the expression of the *gyrA* gene, which was used as an internal reference. Data were calculated according to the $2^{-\Delta\Delta CT}$ method.

2.4.6 Western blotting analysis. The biofilm samples of *S. mutans* treated with SSN, AS*vicR* and SSN-AS*vicR* respectively were prepared as described in 4.4. The biofilm cells were collected by scraping. For the measurement of the DexA and VicR produced, harvested cells were washed and resuspended in 300 μL cold phosphate buffered saline (PBS, pH 7.3). Cells were mechanically disrupted by ultrasonic disruption for three cycles of 20 s. Clear supernatants were collected by centrifugation (13 000 rpm, 2 min, and 4 °C) and protein concentrations were determined using a bicinchoninic acid (BCA) protein assay kit (BioRad, Hercules, CA, USA) according to the manufacturer's instructions.

For western blotting analysis, equal amounts of protein (50 μg) were mixed with 2× SDS-PAGE sample loading buffer (Beyotime Biotech, Shanghai, China) in boiling water for 10 min and loaded on 10% SDS-PAGE gels (Bio-Rad). Proteins were fractionated and then electrotransferred to polyvinylidene fluoride (PVDF) membranes (Biosharp Biotech, Shanghai, China). Membranes were blocked in TSBT buffer (25 mM Tris, 140 mM NaCl, 3 mM KCl, 0.1% Tween 20) containing 5% w/v nonfat dry milk at room temperature for 1 h. The membranes were incubated with purified DexA or VicR-specific polyclonal antibodies (1 : 1000, AbMax Biotechnology, Beijing, China) overnight at 4 °C, washed with TSBT buffer, and incubated with horse-radish peroxidase (HRP)-conjugated goat anti-rabbit secondary antibody (1 : 10 000) for 2 h at room temperature as previously described.[6] Protein immunoreactive bands were visualized using an Immobilon Western Chemiluminescent kit (Millipore, Billerica, MA, USA). The ChemiDoc MP Imaging system (Bio-Rad) was used to detect the signal density of the protein bands.

2.4.7 Electrophoretic mobility shift assays (EMSA). To generate VicR-His-Tag fusion proteins, the ORF was obtained by oligonucleotide synthesis (Sangon Biotech). Next, the NdeI- and XhoI-digested ORF sequences were cloned into pET-21a (Novagen) with His-Tag to yield pET-*vicR*. Plasmids were sequenced and then transformed into *E. coli* BL21, and recombinant proteins were isolated from 500 mL of overnight culture after 3 h of induction with 1 mM IPTG (OD_{600} 0.5). After cell lysis, recombinant proteins were purified by affinity chromatography on Ni^{2+} NTA agarose (Qiagen) as per manufacturer's instructions. The purity/integrity of the purified protein was visualized by Coomassie staining after SDS-PAGE.[4,6,7]

Electrophoretic mobility shift assays (EMSA) were used to determine whether promoter regions of the *dexA* gene were regulated by VicR as previously described.[7] Amplicons of the promoter regions of the *dexA* gene were labeled with FAM (Qingke Biological Technology Co., Ltd, Beijing, China; the primers are listed in ESI† Table S1). Binding reactions of labeled DNA (20 fmol) with recombinant VicR protein (0, 20, 40, 60, and 80 pmol) were carried out in volumes of 20 μL containing 1× binding buffer [100 mM Tris, 500 KCl, 10 mM DTT; pH 7.5], with one-hundred-fold excess of unlabeled DNA fragments (cold DNA) as a competitor.[4] After incubation for 30 min on ice, the reactants were loaded onto non-denaturing 6% acrylamide gels in 0.5× TBE buffer (44.5 mM Tris-HCl, 44.5 mM boric acid, 1 mM EDTA, pH 8.0). Protein–DNA complexes were separated at 4 °C (100 V, 3 h) in 0.5x TBE buffer. The signals were directly detected using the ChemiDoc MP system (Bio-Rad) according to the manufacturer's instructions.

2.5 Cytotoxicity assessment

Human gingival epithelial cells (HGECs) were obtained from clinical samples. The Ethics Committee of West China Hospital of Stomatology approved the use of HGECs in the present study. HGECs were cultured in Dulbecco's modified Eagle medium (DMEM) supplemented with 10% (v/v) heat-inactivated fetal bovine serum (FBS), penicillin (100 U mL^{-1}), and streptomycin (100 μg mL^{-1}) at 37 °C under 5% CO_2 air conditions. For the cytotoxicity assays, HGECs in the logarithmic growth phase were seeded in a 96 well plate at a density of 5000 cells per well overnight. Next, the HGECs were treated with different concentrations (3.6, 14.4, and 28.8 μg mL^{-1}) of SSN-AS*vicR* suspension. After incubation for 24 h, relative metabolic activity was assessed using the Cell Counting Kit-8 (Dojindo, Japan) as previously described.[29] Live/dead staining was performed using the calcein-AM/PI kit (Solarbio, Beijing, China). Fluorescently labeled cells were observed using a fluorescence microscope (Leica, Germany), where the live and dead cells were stained with calcein-AM and PI into green and red, respectively.

2.6 Animal study

To investigate the effects of SSN-AS*vicR* nanoparticles on the formation of dental plaque and cariogenicity *in vivo*, a rat model was used as previously described.[24,30,31] Animal experiments

were reviewed and approved by the Ethics Committee of West China Hospital of Stomatology, Chengdu, China (Permit number: WCHSIRB-D-2021-336). Twenty-four specific-pathogen-free Wistar rats (male, 3 weeks of age) were included (Experimental Animal Center of Public Health, Sichuan University, Chengdu, China). Before the *S. mutans* inoculation, rats were randomized into four experimental groups: UA159 as a positive control, SSN group, AS*vicR* plasmid group, and SSN-AS*vicR* group (n = 6 rats per group). SPF (specified pathogen-free) animals were housed, 6 rats per cage in a room on a 12 : 12 light/dark cycle. On days 1 to 7, each rat was infected orally with 200 μL of *S. mutans* mid-exponential phase (1×10^8 cells per CFU). The animals received both a cariogenic (sucrose-rich) diet and 5% sucrose water. The cariogenic diet (Trophic Animal Feed High-Tech Co. Ltd, China; NO. TP100352D20) comprises of milk powder, sucrose, starch, wheat flour and protein powder, which contains 56% sucrose. Sugar drinks were given using sterile water containing 5% sucrose. For treatment, a sterile cotton bud (Labor Import) was used to swab the rat teeth with 200 μL of SSN (1 mg mL^{-1}), AS*vicR* plasmid (0.12 mg mL^{-1}) or SSN-AS*vicR* (1 mg mL^{-1}) suspensions respectively on days 1 to 14 as per our recently published study.[17] Rats were weighed once a week and then their physical appearance was routinely recorded. On day 28, the animals were sacrificed by CO_2 asphyxiation. The lower jaws were aseptically removed and divided into two pieces. After sonication in a PBS bath, the lower jaws were dissected and immersed in 10% buffered formalin phosphate for 48 h. The researchers were blinded to the group analyzed. The teeth were observed under a stereomicroscope and caries were scored according to a modified Keyes score.[32,33] For micro-CT reconstruction, the mandibular samples were scanned by micro-CT at 7 μm voxels with a resolution of 500 projections/180°. The total scanning time of each sample was 14.3 minutes. After scanning, the images were obtained using Scco Evaluation software (Scco Medical AG).

In addition, another group of rats (n = 4 rats) was used to verify the biological genetic safeties of SSN-AS*vicR*. On days 1 to 3, each rat was infected orally with 200 μL of the mid-exponential phase bacterial suspension that contained the *Streptococcus mutans* UA159 strain, *Streptococcus gordonii*, and *Streptococcus sanguis*. Then, a sterile cotton bud was used to swab the molars of the rats with 200 μL of SSN-AS*vicR* suspension. Swabs were used to collect the salivary samples from the rats' mouth before and five hours after SSN-AS*vicR* treatment. The samples were soaked in DNA/RNA Shield Reagent (ZYMO Research) prior to DNA extraction. Then, we followed the manufacturer's protocol for DNA extraction. The extracted DNA was amplified with universal bacterial primers 8F (5′-AGAGTTTGATCATGGCTCAG-3′) and 1492R (5′-CGGTTACCTTGTTACGACTT-3′) to amplify the full length of the 16S rRNA gene. To avoid errors during cluster identification because of the high similarity of bases across all amplicons, we tagged a 24 bp barcode to forward primers. The 20 μL PCR volume contained 10 ng of extracted DNA and 0.3 μM of primers with Kodaq 2× PCR MasterMix (G497, Applied Biological Materials Inc.). PCR was carried out with an activation step at 95 °C for 3 min followed by 10 touchdown cycles at 95 °C for 10 s, 65 °C (decrease of 1 °C for each cycle) for 20 s, and 68 °C for 90 s, followed by 20 cycles at 95 °C for 10 s and 68 °C for 90 s and a final elongation for 7 min. Amplifications were quantified using a Qubit dsDNA HS Assay Kit (Q32854, Thermo Fisher Scientific) on a Tecan F200 luminescent plate reader, and samples were pooled to equimolar amounts of DNA. The library was prepared as recommended by Nanopore (SQK-LSK109, Oxford Nanopore Technologies, ONT) and loaded on a GridION × 5 flow cell (FLO-MIN106 R9.4.1, Oxford Nanopore Technologies) for a 72 h sequencing protocol using MinKNOW software at Rhonin BioSciences Company (Chengdu, China).

2.7 The effects of pDL278 plasmid containing AS*vicR* on *S. gordonii* and *S. sanguinis*

The *S. gordonii* and *S. sanguinis* strains were provided by the State Key Laboratory of Oral Diseases (Sichuan University, Chengdu, China). *S. gordonii* and *S. sanguinis* strains were routinely grown in brain heart infusion (BHI) media overnight at 37 °C anaerobically (90% N_2, 5% CO_2, and 5% H_2). Then, *S. gordonii* and *S. sanguinis* suspensions were diluted into fresh BHI media at a 1 : 20 ratio and cultured into optical density at 600 nm [OD_{600}] 0.2. For the transformation, the competence stimulating peptide (CSP) was added to the *S. gordonii* and *S. sanguinis* suspension cultures to achieve a final concentration of 1 μg mL^{-1}. Recombinant pDL278 plasmid containing AS*vicR* were simultaneously added to the cultures and incubated for 60 min. *S. gordonii*-AS*vicR* and *S. sanguinis*-AS*vicR* were isolated using BHI plates containing 1000 μg mL^{-1} spectinomycin for selection and incubated for 48 h at 37 °C anaerobically (90% N_2, 5% CO_2, and 5% H_2).

The transcription analyses of *S. gordonii*-AS*vicR* and *S. sanguinis*-AS*vicR* strains respectively were prepared as described in 4.5. For planktonic cultures, *S. gordonii*-AS*vicR* and *S. sanguinis*-AS*vicR* cultures were grown overnight to the mid-exponential phase in BHI medium. The suspensions of *S. gordonii*-AS*vicR* and *S. sanguinis*-AS*vicR* were followed by diluting 100 μL culture into 2 mL of fresh BHI. Total RNAs of *S. gordonii*-AS*vicR* and *S. sanguinis*-AS*vicR* planktonic cultures were extracted using a MasterPure RNA purification Kit (Epicentre, MD, USA). The planktonic cells were collected by centrifugation (4500 rpm, 4 °C) for 15 min, washed with PBS buffer and resuspended in tissue and cell lysis solution (MasterPure RNA purification Kit). The genomic DNA was removed by digestion with Turbo RNase-free DNase I (Ambion, Austin, TX, USA) according to the manufacturer's instructions. RNA samples were reverse transcribed to complementary DNA (cDNA) using random 6 mers with the RevertAid First Strand cDNA Synthesis Kit (Thermo Scientific, MA, USA). Real-time PCR was carried out as described in 4.5. Primers used in real-time PCR reactions are shown in ESI,† Table S1 and were obtained commercially (Sangon Biotech, Shanghai, China). Threshold cycle values (CT) were quantified and the expression of each gene was normalized relative to the expression of the 16sR genes of *S. gordonii* and *S. sanguinis*, which was used as an internal reference. Data were calculated according to the $2^{-\Delta\Delta CT}$ method.

2.8 Data analysis

Statistical analyses of the data were performed using SPSS 16.0 (SPSS Inc., Chicago, IL, USA). Shapiro–Wilk tests were conducted to examine the normal distribution of the experimental data, and Bartlett's tests were performed to assess the homogeneity of variances. For parametric testing, one-way analysis of variance (ANOVA) was used to detect the significant effects of variables followed by the Student–Newman–Keuls test to compare the means of each group. For nonparametric testing, the Kruskal–Wallis test and least significant difference (LSD) multiple comparisons were used for comparison. A value of $p < 0.05$ was considered statistically significant.

3. Results

3.1 Materials characterization of SSN and SSN-ASvicR

The morphology of SSN-AS*vicR* nanoparticles was greatly affected by the dispersion liquid (Fig. 1A). The M_w of degraded starch was 21 112 g mol^{-1}, and the molecular weight distribution is shown in ESI,† Fig. S2. Zeta potential measurements demonstrated that the mean surface charges of AS*vicR*, SSN-AS*vicR*, SSN-1, SSN-2, and SSN-3 were −32.9 mV, −8.1 mV, 55.9 mV, 29.6 mV, and 25.2 mV, respectively (Fig. 1B). The grafting of spermine onto the starch chain was verified by the results of FTIR. Additional signal peaks were detected in the spectra of SSN-1, SSN-2, and SSN-3, such as the amide I band associated with the C=O stretching vibration at 1699 cm^{-1}, the amide II band arising mainly from the in-plane N–H bending vibration at 1548 cm^{-1}, and the amide III band located at 1264 cm^{-1} (Fig. 1C).[34] The ^{1}H NMR analysis results further confirmed the successful conjugation of spermine (Fig. 1D). In addition to the peaks belonging to the starch backbone, which appeared at δ = 5.38 ppm and δ = 3.5–3.9 ppm, new peaks were observed at δ = 1.1–3.3 ppm, and were assigned to the protons on the spermine chains. Table 1 shows the results of quantitative analysis of EA. Among the three SSN materials, SSN-1 displayed the highest amount of grafted spermine. As the grafting amount increased, the grafting efficiency decreased accordingly.

3.2 The binding capacity, biodegradation behavior, and protective effect of the SSN

SSN-1 could reduce the migration of the AS*vicR* plasmid at or above a w/w ratio of 2, whereas clear AS*vicR* plasmid bands could be observed in the agarose gel for SSN-2 and SSN-3, thus indicating that their AS*vicR* plasmid binding abilities were weaker than that of SSN-1 (Fig. 2A). For this reason, SSN-1 was selected for SSN-AS*vicR* fabrication in this study.

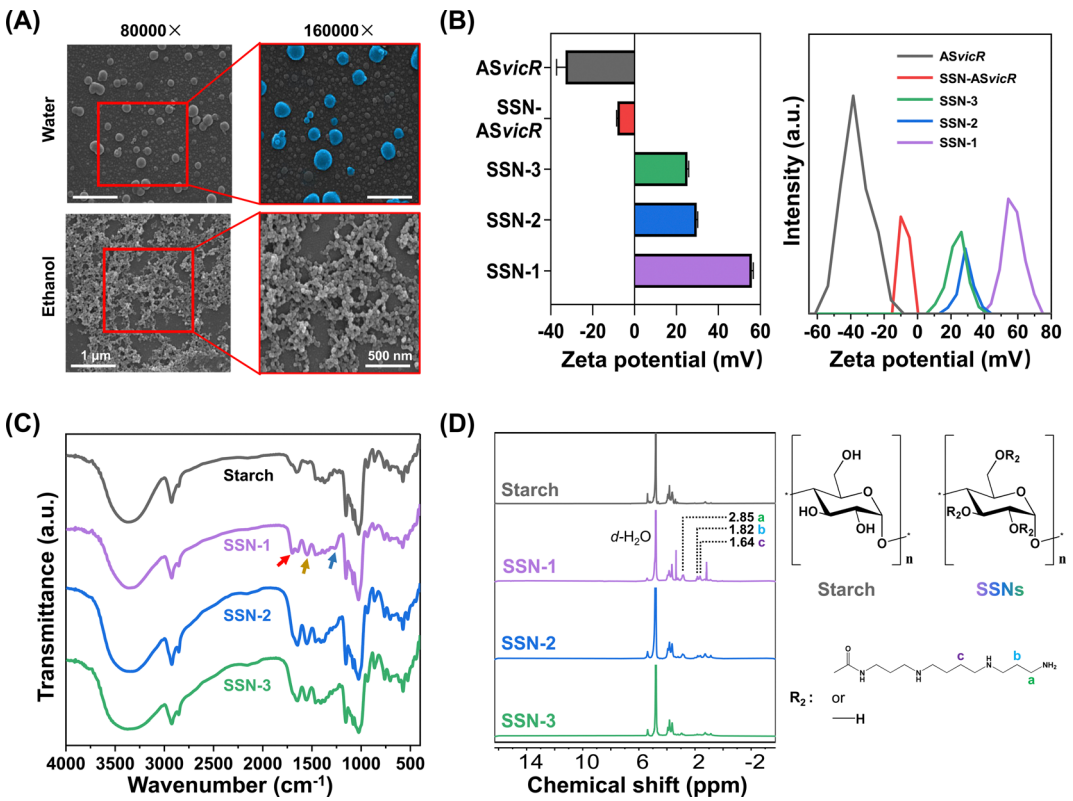

Fig. 1 Materials characterization of SSN materials and SSN-AS*vicR*. (A) SEM images of SSN-AS*vicR* nanoparticles dispersed in ethanol and deionized water (swollen nanoparticles are colored in pseudo blue). (B) The zeta potential of AS*vicR* plasmid, SSN materials, and SSN-AS*vicR* (left: mean and standard deviation of zeta potential in each group; right: typical potential-intensity curves). (C) Fourier transform infrared spectra of degraded starch and SSN materials. The red, yellow, and blue arrows represent additional signal peaks detected on the spectra of SSN materials at 1699 cm^{-1}, 1548 cm^{-1}, and 1264 cm^{-1}, respectively. (D) ^{1}H NMR spectra of degraded starch and SSN materials. Protons on the spermine chain were labelled by colored lowercase letters and assigned to the additional signal peaks at δ = 1.1–3.3 ppm on the spectra of SSN materials.

Table 1 Quantification of spermine on the grafts as determined by elemental analysis (mean ± SD, n = 4)

	Nitrogen content (%)	Molar ratio of spermine to glucose unit	Grafting efficiency of spermine (%)	Weight percent of spermine (%)
SSN-1	4.21 ± 0.77	0.15 ± 0.03	29.23 ± 6.34	15.10 ± 2.77
SSN-2	3.29 ± 0.72	0.11 ± 0.03	43.79 ± 10.97	11.79 ± 2.59
SSN-3	2.56 ± 0.45	0.08 ± 0.02	49.50 ± 9.66	9.20 ± 1.63

Subsequently, SSN-AS*vicR* was mixed with α-amylase in a water bath to analyze the biodegradable properties. The AS*vicR* plasmid bands were detected in all of the groups, and the dose of α-amylase was positively correlated with the clearness of the bands, thus indicating that the AS*vicR* plasmid was released due to the hydrolyzation of the starch chain in SSN-AS*vicR* (Fig. 2B). After DNase I treatment, the naked AS*vicR* plasmid was completely degraded and could not be detected in the gel (Fig. 2C, Lane 4). In contrast, the AS*vicR* plasmid bound with the SSN was still retained in the well (Fig. 2C, Lane 2). A schematic diagram of enzymatic digestion of SSN-AS*vicR* by α-amylase or DNase I is shown in Fig. 2D.

3.3 Biocompatibility and transformation efficiency of SSN-ASvicR

As shown in Fig. 2E and F, the cell viability and morphology of human gingival epithelial cells (HGECs) treated with the SSN-AS*vicR* suspension showed no significant difference from those of the negative control. The cells were stained green (live cells), and few red-stained cells (dead cells) could be observed. The CCK-8 assay showed that HGEC cells treated with the SSN-AS*vicR* suspension did not show a statistically significant difference from that of the negative control group (Fig. 2G), thus suggesting that SSN-AS*vicR* had favorable cytocompatibility. To ensure the transformation of the AS*vicR* plasmid into *S. mutans* cells, the

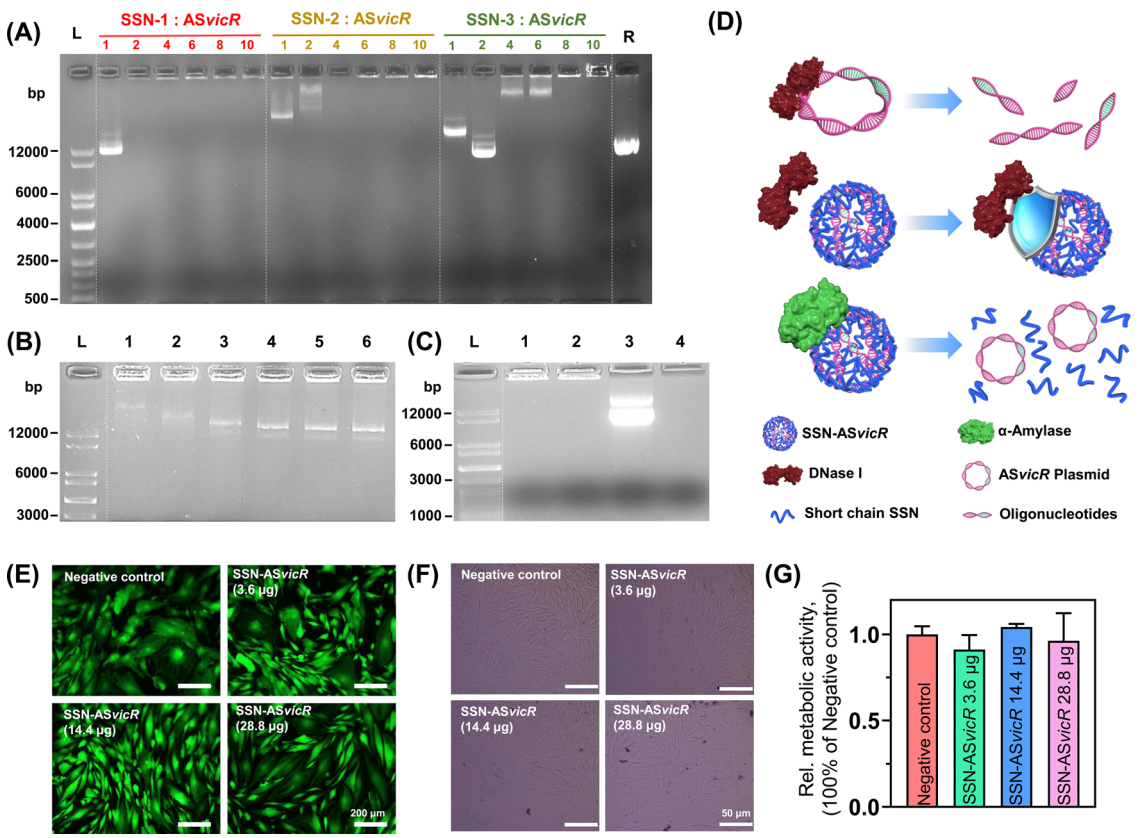

Fig. 2 The biological characteristics of SSN. (A) The loading capacities of SSN-1, SSN-2, and SSN-3. SSN materials were mixed with AS*vicR* plasmids at mass ratios of 1, 2, 4, 6, 8, and 10. The uppercase L and R represent ladder and reference (AS*vicR* plasmid), respectively. (B) AS*vicR* plasmids were released after α-amylase treatment due to the hydrolyzation of the starch chain in SSN-AS*vicR* (Lane 1 : 30 μg SSN-AS*vicR* + 25 μg α-amylase; Lane 2 : 30 μg SSN-AS*vicR* + 75 μg α-amylase; Lane 3 : 30 μg SSN-AS*vicR* + 125 μg α-amylase; Lane 4 : 30 μg SSN-AS*vicR* + 175 μg α-amylase; Lane 5 : 30 μg SSN-AS*vicR* + 225 μg α-amylase; Lane 6 : 30 μg SSN-AS*vicR* + 275 μg α-amylase). (C) SSN-AS*vicR* protected the AS*vicR* plasmid in the presence of DNase I (Lane 1: SSN-AS*vicR*; Lane 2: SSN-AS*vicR* + DNase I; Lane 3: AS*vicR* plasmid; Lane 4: AS*vicR* plasmid + DNase I). (D) Schematic diagram of enzymatic digestion of SSN-AS*vicR* by α-amylase or DNase I. (E) Representative live/dead staining images of human gingival epithelial cells treated by SSN-AS*vicR*. Live and dead cells were stained green and red, respectively. (F) Light microscope figures of human gingival epithelial cells treated with SSN-AS*vicR*. (G) Relative metabolic activities of human gingival epithelial cells treated with SSN-AS*vicR*.

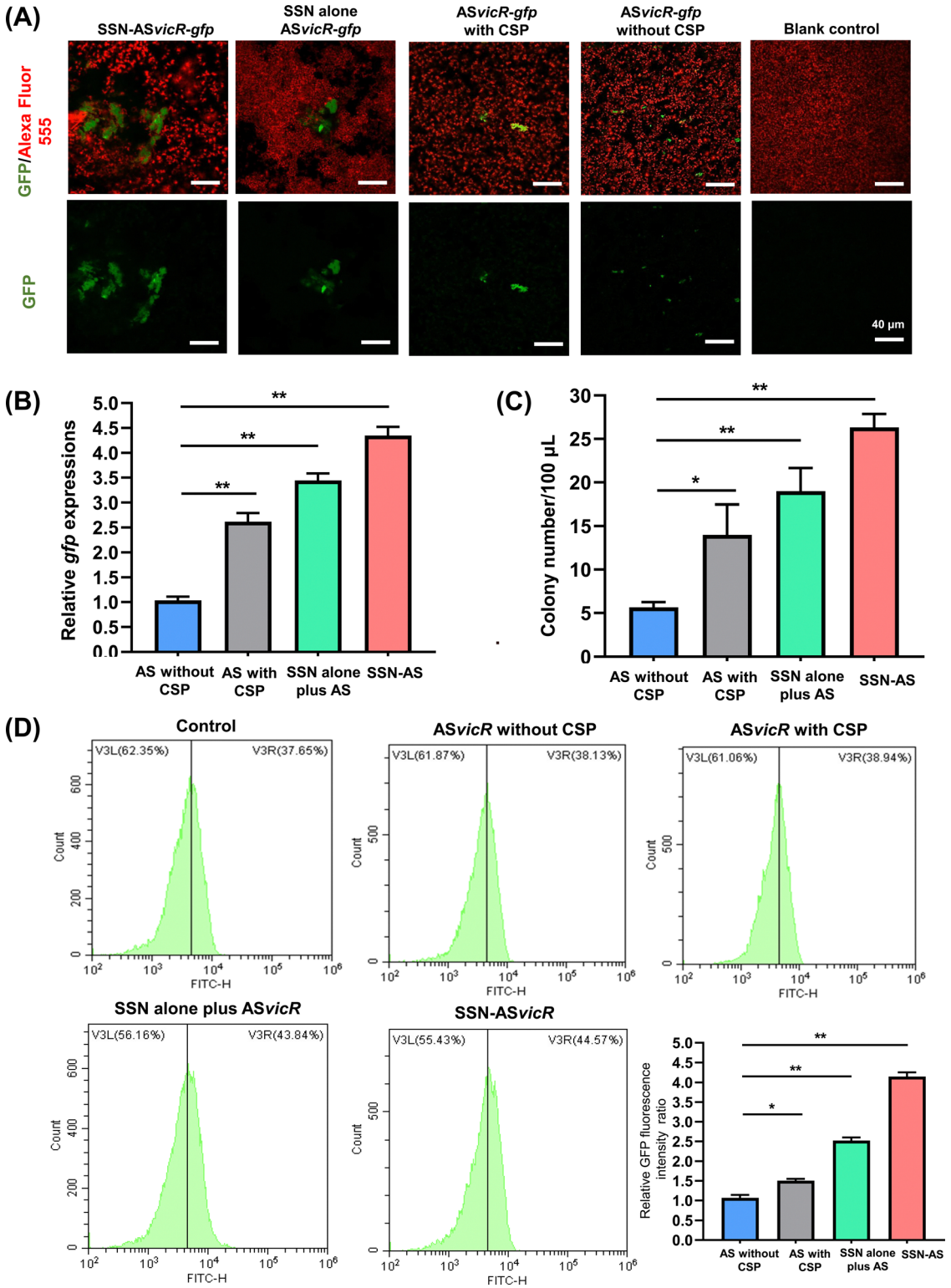

Fig. 3 Suppression effect of SSN-AS*vicR* on biofilm organization of *S. mutans*. (A) Transformation efficiency of the SSN-AS*vicR* labelled with green fluorescent protein (GFP) was evaluated and *S. mutans* expressed GFP after SSN-AS*vicR-gfp*, AS*vicR-gfp* with CSP, AS*vicR-gfp* without CSP or SSN plus AS*vicR-gfp* treatment. The cell walls of *S. mutans* were stained red by Alexa Fluor 555. (B) Relative gene transcription levels analyzed by quantitative RT-PCR. The *S. mutans* biofilm cells were treated with SSN, AS*vicR* and SSN-AS*vicR* respectively. *S. mutans* UA159 parent strain was used as a control group. The asterisks indicate significant differences in relation to UA159. *gyrA* was set as the internal control with an expression level of 1.0 (mean ± standard deviation, $*P < 0.05$, $**P < 0.01$, $n = 5$). (C) The colony number on selective plates of 100 μL bacterial suspensions after SSN-AS*vicR-gfp*, AS*vicR-gfp* with CSP, and AS*vicR-gfp* without CSP and SSN plus AS*vicR-gfp* treatment (mean ± standard deviation, $*P < 0.05$, $**P < 0.01$, $n = 5$). (D) The flow cytometry for bacterial suspensions after SSN-AS*vicR-gfp*, AS*vicR-gfp* with CSP, and AS*vicR-gfp* without CSP and SSN plus AS*vicR-gfp* treatment. Untreated *S. mutans* was set as blank control. The fluorescence above the background level was calculated, and relative GFP fluorescence intensity ratios were calculated (mean ± standard deviation, $*P < 0.05$, $**P < 0.01$, $n = 3$).

recombinant AS*vicR* plasmid was labeled with a *gfp* tag. As shown in Fig. 3A, *S. mutans* cell walls were stained red with Alexa Fluor 555, and GFP was observed (green fluorescence). The quantification of the *gfp* gene expression *via* quantitative RT-PCR and the transformation assays with selective plating cell counting indicated that the transformation efficiency of SSN-AS*vicR* transformation was four times that of the naked AS*vicR* plasmid (Fig. 3B and C). Additionally, the flow cytometry assay indicated that the SSN-AS*vicR* transformation efficiency was the highest (Fig. 3D).

3.4 Suppression effect of SSN-ASvicR on biofilm organization of *S. mutans*

The SEM results showed that the untreated *S. mutans* were densely packed with an enriched extracellular matrix (ECM), whereas SSN-AS*vicR*-treated bacteria appeared to be scattered

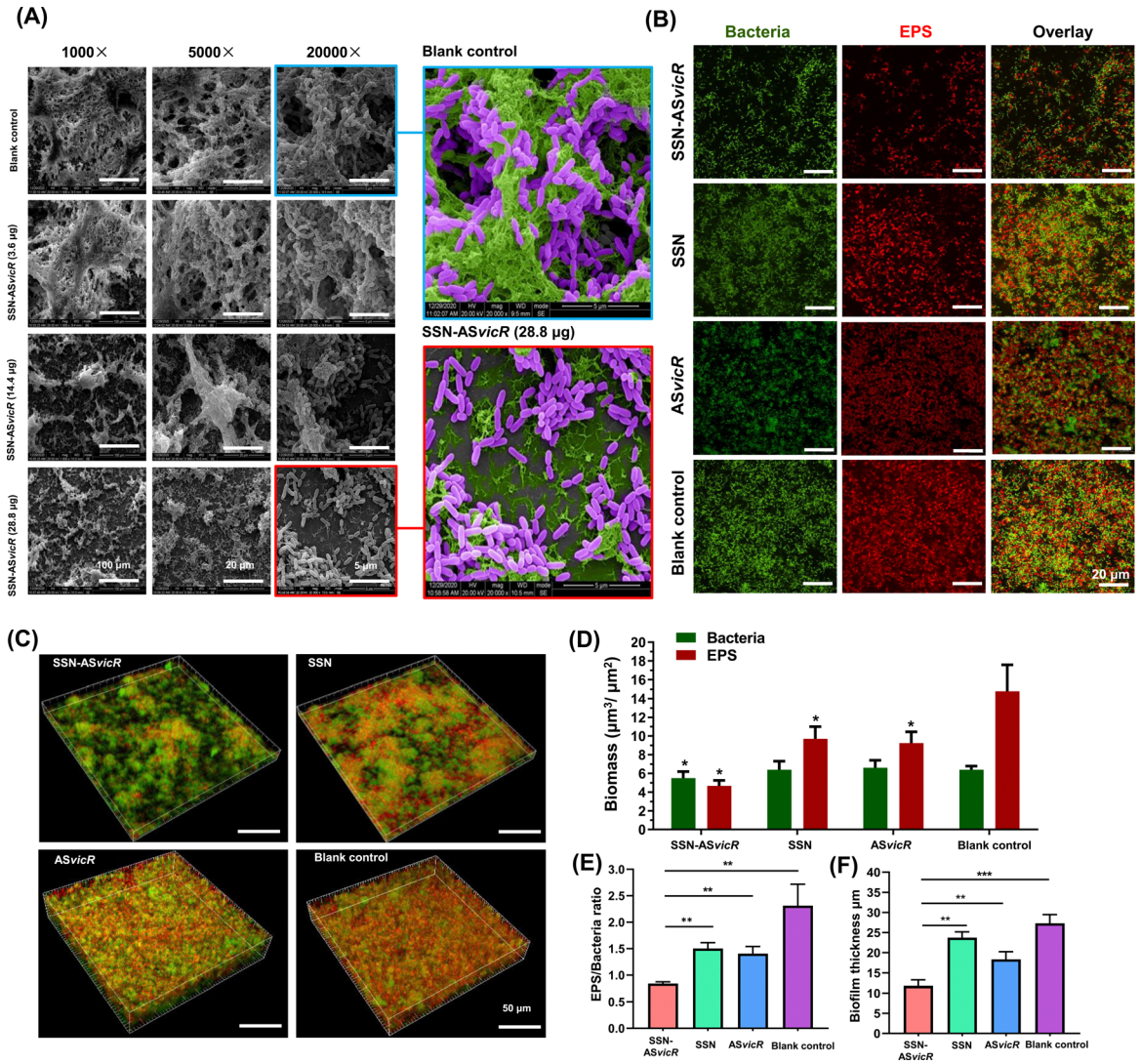

Fig. 4 EPS production in biofilms of *S. mutans* treated with SSN-AS*vicR*. (A) Representative SEM images of *S. mutans* biofilm treated with SSN-AS*vicR* every 4 h to imitate mouth rinse; SSN-AS*vicR* was added to the culture in each well every 4 h during 12 h incubation and the biofilms were formed in the presence of SSN-AS*vicR* from 12 h to 24 h incubation at 37 °C anaerobically. Untreated *S. mutans* was set as blank control. (B) Confocal laser scanning microscopy (CLSM) images of *S. mutans* biofilm treated with SSN, AS*vicR*, and SSN-AS*vicR*. For SSN-AS*vicR* treatment, 28.8 μg of SSN-AS*vicR* were added to the culture in each well every 4 h during 12 h incubation and the biofilms were formed in the presence of SSN-AS*vicR* from 12 h to 24 h incubation at 37 °C anaerobically (90% N_2, 5% CO_2, and 5% H_2). For AS*vicR* treatment, 3.2 μg of AS*vicR* plasmid were added to the culture in each well every 4 h during 12 h incubation and the biofilms were formed in the presence of AS*vicR* from 12 h to 24 h incubation at 37 °C anaerobically. For SSN treatment, 25.6 μg of SSN were added to the culture in each well every 4 h during 12 h incubation and the biofilms were formed in the presence of the SSN from 12 h to 24 h incubation at 37 °C anaerobically. Untreated *S. mutans* was set as blank control. The EPS was stained red, and bacterial cells were stained green. (C) Three-dimensional fluorescence images of *S. mutans* biofilms. (D) The EPS biomass and the cell biomass in *S. mutans* biofilms; the asterisks indicate significant differences in relation to the blank control (*$P < 0.05$, **$P < 0.01$, $n = 9$). (E) The ratios of EPS/bacteria in biofilms (*$P < 0.05$, **$P < 0.01$, $n = 9$). (F) The thicknesses of biofilms were also variable between the treatments (*$P < 0.05$, **$P < 0.01$, $n = 9$).

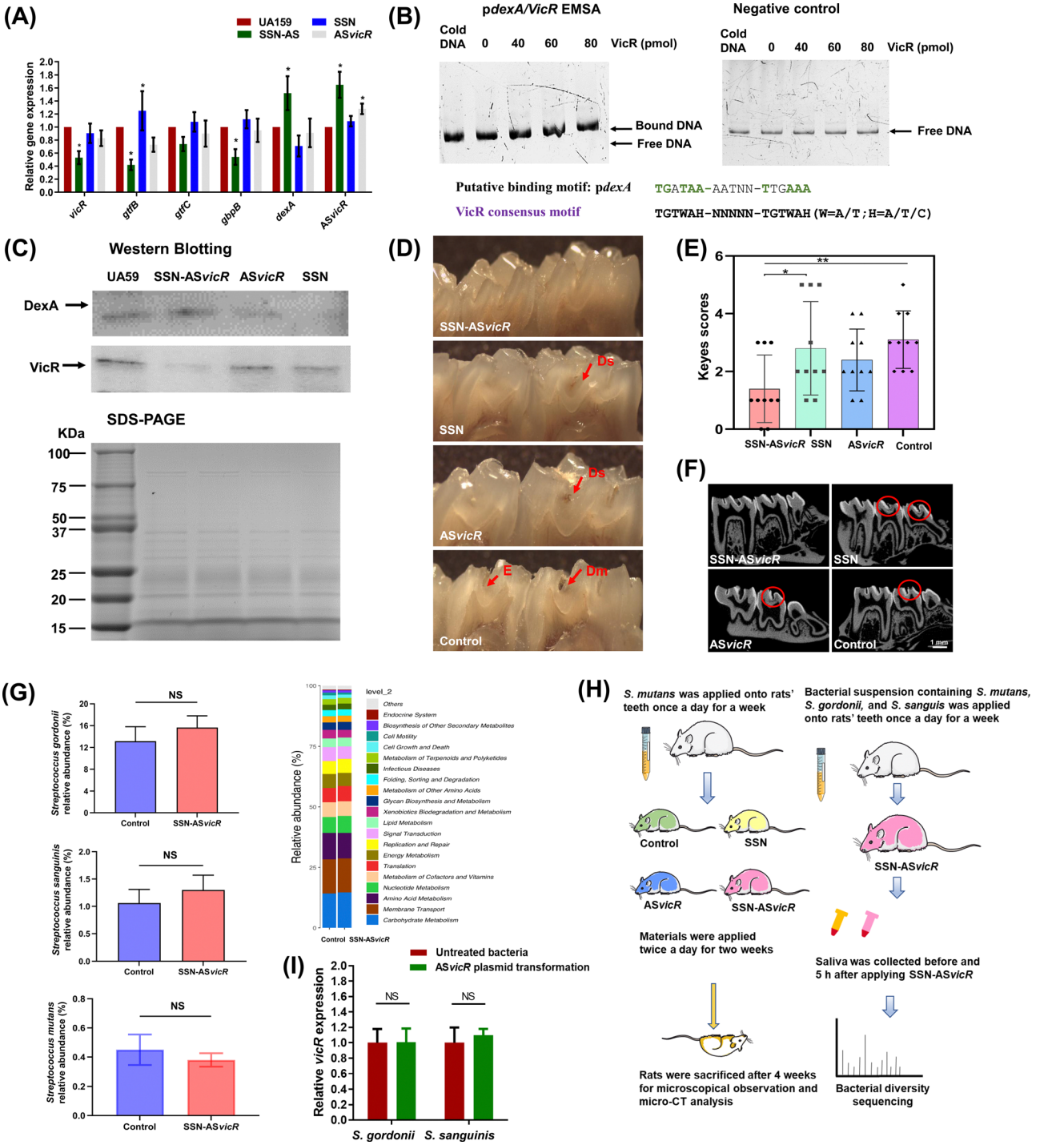

Fig. 5 Transcriptional analysis and animal experiments of *S. mutans* treated with SSN-AS*vicR*. (A) Relative gene transcription levels analyzed by quantitative RT-PCR. The *S. mutans* biofilm cells were treated with SSN, AS*vicR* and SSN-AS*vicR* respectively. *S. mutans* UA159 parent strain was used as the control group. The asterisks indicate significant differences in relation to UA159. *gyrA* was set as the internal control with an expression level of 1.0 (mean ± standard deviation, $*P < 0.05$, $n = 9$). (B) Electrophoretic mobility shift assays (EMSA) demonstrated the potential interactions between VicR and candidate target gene *dexA*. Regarding the EMSA negative control, a DNA fragment the same size as the *dexA* promoter and a similar AT:GC mole ratio, but missing the VicR consensus binding sequence, was used to rule out non-specific binding. The cold (unlabeled) promoter DNAs were used to out-compete VicR-specific binding. The binding was reduced in the presence of excess non-labelled DNA suggesting specificity of VicR binding. The promoter regions of the *dexA* gene were analyzed *via* online program BPROM – Prediction of bacterial promoters (**https://linux1.softberry.com/**) and one predicted promoter had been found. The predicted promoter sequences indicated that the *dexA* promoter region includes a VicR consensus binding sequence. (C) The production of VicR and DexA evaluated by western blotting (upper panel); Coomassie brilliant blue staining was applied to show the total proteins in different groups. (D) Stereomicroscopic images of pit and fissure caries on the teeth of rats (enamel (E), dentinal (Dm), and extensive dentinal (Ds)). (E) The caries scores assessed by a modified total Keyes' counting method ($*P < 0.05$, $n = 6$). (F) Micro-CT analysis of pit and fissure caries. (G) The abundances of *S. mutans*, *S. gordonii* and *S. sanguinis* were compared in control and test groups, indicating that there was no significant difference (mean ± standard deviation, $P > 0.05$, $n = 4$). KEGG annotation statistics for transcriptome analysis. (H) The experimental flowchart of animal study. (I) The pDL278 plasmid containing AS*vicR* was transformed into *S. gordonii* and *S. sanguinis* respectively. The RTq-PCR results indicated that the expression of the homologous *vicR* gene in both *S. gordonii* and *S. sanguinis* was not affected by transformation of the pDL278 plasmid containing AS*vicR* (mean ± standard deviation, $P > 0.05$, $n = 9$).

with reduced ECM interspersed among empty areas (Fig. 4A). Moreover, the CLSM observation showed that the EPS production of the SSN-treated, AS*vicR*-treated, and SSN-AS*vicR*-treated *S. mutans* decreased compared to that of the untreated *S. mutans* (Fig. 4B and C). Interestingly, we found that EPS biomass was variable between the treatments, and the cell biomass in the SSN-AS*vicR* group was changed compared with the untreated *S. mutans* (Fig. 4D). Further quantitative analysis showed that the EPS/bacteria ratios of the SSN-AS*vicR*-treated *S. mutans* biofilm were significantly lower than those of the AS*vicR*-treated biofilm (Fig. 4E). The thickness of biofilms was also variable between the treatments, indicating that the biofilm of the SSN-AS*vicR* group was the lowest (Fig. 4F).

3.5 Mechanism analyses of the suppression effect of SSN-AS*vicR* on the biofilms of *S. mutans*

Quantitative RT-PCR assays showed that *S. mutans* biofilm cells treated with SSN-AS*vicR* were different from those observed after treatment with naked AS*vicR*. Interestingly, there was upregulation of *gtfB* in *S. mutans* treated with SSN alone (Fig. 5A and Fig. S3, ESI†). The transcription levels of the *vicR*, *gtfB/C*, and *gbpB* genes in the SSN-AS*vicR*-treated group exhibited the lowest values. Furthermore, EMSA was performed on the promoter regions of the *dexA* gene, which demonstrated that the VicR protein was directly bound to the *dexA* promoter regions (Fig. 5B). Western blot analysis of VicR and DexA proteins revealed that VicR expression levels were decreased in the AS*vicR*-treated and SSN-AS*vicR*-treated biofilms (Fig. 5C). The quantitative RT-PCR assays indicated that *dexA* transcription was significantly decreased in a *vicK* knockout mutant (Fig. S4, ESI†), which would strengthen the proposal that *dexA* is directly regulated by VicR as well as VicRK TCS.

3.6 *In vivo* effects of SSN-ASvicR on the cariogenicity of *S. mutans* and oral microbiota homeostasis

The treatments were applied daily for two weeks to investigate the effects on the oral microbiota and incidence of caries after *S. mutans* colonization. As shown in Fig. 5D, a lower cariogenic incidence was observed in dentinal (Dm) and extensive dentinal (Ds) regions of the rat teeth treated with AS*vicR* and SSN-AS*vicR*. Particularly, the SSN-AS*vicR*-treated rat teeth showed the lowest cariogenic incidence, which was calculated by using the modified Keyes' counting method (Fig. 5E and Table S2, ESI†). Micro-CT analysis showed that pit and fissure caries occurred in rat teeth without SSN-AS*vicR* treatment (Fig. 5F), which was consistent with the results of Keyes' counting method. To address the potential effects of AS*vicR* on commensal *streptococci*, the abundances of *S. mutans*, *S. gordonii* and *S. sanguinis* were compared in the control and test groups, which indicated that there was no significant difference. In addition, KEGG pathway impact analysis demonstrated similar functional prediction results of metabolic pathways between control and SSN-AS*vicR* treated groups (Fig. 5G). The experimental flowchart of animal study is listed in Fig. 5H. We transformed the pDL278 plasmid containing AS*vicR* into *S. gordonii* and *S. sanguinis*. The quantitative RT-PCR results indicated that the expression of the homologous *vicR* gene in both *S. gordonii* and *S. sanguinis* was not affected by transformation of the pDL278 plasmid containing AS*vicR* (Fig. 5I).

4. Discussion

In the present study, SSN materials were developed by grafting spermine onto the starch molecule *via* CDI activation. Due to its excellent binding capacity, SSN-1 was selected to effectively encapsulate the AS*vicR* plasmid. The morphology of SSN-AS*vicR* nanoparticles dispersed in deionized water was larger and more uneven in size than those dispersed in ethanol, which could be explained by the swelling effect. The presence of nitrogen in SSN materials was confirmed by EA, signifying the successful grafting of spermine onto the starch chain.[35] This could be further verified by the results of FTIR and ^{1}H NMR, demonstrated by the additional signal peaks on the spectra.[16,36] With an increase in the grafting amount of spermine, we observed a decrease in grafting efficiency (Table 1). This might be explained by the steric hindrance and electrostatic repulsion phenomenon in polymer grafting.[37] The zeta potential results suggest the possible binding mechanism between the SSN materials and the AS*vicR* plasmid. Before binding, the SSN materials exhibited a distinct positive charge (55.9 mV, 29.6 mV, and 25.2 mV), while the AS*vicR* plasmid carried a noticeable negative charge (−32.9 mV). The zeta potential of the resulting complex (SSN-AS*vicR*) lies between the two (−8.1 mV), indicating that the SSN and AS*vicR* may bind together through electrostatic adsorption. The favorable cytocompatibility of SSN-AS*vicR* may be attributed to the raw materials used for SSN fabrication; specifically, starch is a naturally available and environmentally friendly material with excellent biocompatibility, and spermidine is an endogenous polyamine that is beneficial in extending lifespans through epigenetic modifications and necrosis suppression.[38]

To ensure the transformation of the AS*vicR* plasmid into *S. mutans* cells, we chose a green fluorescent protein (GFP) as a model protein for investigation,[39] and *S. mutans* cell walls were marked *via* Alexa Fluor 555.[40] Regarding the treatment with SSN-AS*vicR* and its effects on promoting a gene transcript profile, it has been reported that the source of carbohydrate significantly impacts the stochastic behaviors that can induce competence in *S. mutans*.[41,42] In the present study, the SSN could be bio-suitably hydrolyzed by the endogenous α-amylase of *S. mutans*,[43] which may stimulate the progression to the competent state. Taken together, we speculated that carbohydrate sources not only induce genetic competence but also alter the expression of EPS-related genes.

The results of the SEM observation and CLSM analysis revealed that SSN-AS*vicR* could significantly reduce the *S. mutans* biofilm due to its inhibitory effect on EPS production. *Via* complementary base pairing, AS*vicR* was able to form a double-stranded structure with *vicR* mRNA, thereby inhibiting the transcription and translation of the *vicR* gene.[6,7] Because two component systems (TCSs)[44] are widely present in most

lower eukaryotes and prokaryotes, AS*vicR* can target the *S. mutans* VicRK TCS without affecting mammalian cells. Etiologically, EPS plays a key role in the development of dental caries by promoting bacterial adhesion and aggregation.[45] As the long-term application of antibiotics may induce drug resistance and dysbacteriosis,[46] the EPS reduction in cariogenic biofilms is beneficial for the prevention and treatment of dental caries. With fewer adverse complications, SSN-AS*vicR* nanoparticles may be a promising alternative or supplement to the currently used antibiotics.

Our previous study indicated that the expression of the AS*vicR* RNA transcript was elevated in planktonic cultures and repressed during biofilm growth.[6] In the present study, we detected changes in AS *vicR* in planktonic and biofilm cultures (Fig. S3, ESI†), which indicated that the increase in AS*vicR* expression in *S. mutans* treated with SSN-AS*vicR* in the planktonic state was greater than that in the biofilm state. We speculated that the SSN system improves the efficiency of AS*vicR* transformation by inducing genetic competence, especially in the planktonic state. Regarding the SSN-AS*vicR* nanoparticle stability, we detected the quantity of released nucleic acid (Fig. S5, ESI†) from the SNN-AS*vicR* complex at RT (room temperature) and 4 °C as well as with or without FBS (10% FBS representing *in vitro* and *in vivo* conditions respectively).

Interestingly, the SSN alone inhibited EPS/bacteria ratios, and treatment with the SSN alone also reduced VicR expression. One possible explanation was consistent with the results of our previous study,[6] which showed that the transcripts of AS*vicR* were elevated when *S. mutans* biofilm cultures were complemented with sucrose or glucose. As the SSN can be hydrolyzed by endogenous α-amylase of *S. mutans* and can serve as a carbohydrate source, *S. mutans* treated with the SSN alone likely reduced VicR expression and inhibited EPS production.[6,7,24] Dental caries is a complex process that is also associated with other bacteria. The dynamic balance between commensals and opportunistic pathogens was disrupted, which causes microbial community shifts and disrupts tooth-enamel mineral homeostasis.[47,48] The SSN nanoparticles have a slight inhibitory effect on the *Enterococcus faecalis* or *Streptococcus sanguis* (Fig. S6 and S7, ESI†). Another possible explanation was that the SSN (as a positively charged surface material) is supposed to capture or affect bacteria,[49] thus warranting further investigation.

In this study, we found that the *vicR*, *gtfB/C*, and *gbpB* expression levels were significantly downregulated by AS*vicR* and SSN-AS*vicR* treatment. The upregulation of *gtfB* in *S. mutans* treated with the SSN alone was consistent with the results of a previous study,[4] which indicated that the expression of the *gtfB* gene was elevated when *S. mutans* was in biofilms supplemented with sucrose. In contrast, the *dexA* gene expression was significantly elevated in the SSN-AS*vicR*-treated group. We previously reported that *dexA*-encoded dextranase (DexA) could partially inhibit the synthesis of and promote the digestion of glucans and eventually cause the breakdown of biofilm organization.[50] As the *dexA* gene expression increased in the SSN-AS*vicR*-treated group, we speculated that VicR negatively regulates the *dexA* gene transcription and that SSN-AS*vicR* represses EPS biosynthesis by digesting glucans. As a VicR-binding box was found in the *dexA* promoter, further investigations are needed to explore the interactions of the specific VicR-binding box in the *dexA* promoter and the VicR protein.

Hu *et al.* sampled saliva at 10 to 60 min intervals to track the high-resolution microbiome dynamics during the course of human eating activities for 5 days.[51] Indeed, it is uncertain whether the abundance of streptococcal species analyzed only 5 h after SSN-AS*vicR* treatment has biological significance, and further investigations are needed. Regarding the high degree of conservation of *vicR* genes, there is a 71.5% similarity of *vicR* genes between *S. mutans* and *S. gordonii*, as well as a 72.6% similarity of *vicR* genes between *S. mutans* and *S. sanguinis*. However, there is only a 23.9% similarity between *S. mutans* AS*vicR* and the *S. gordonii vicR* gene, as well as only a 24.9% similarity between *S. mutans* AS*vicR* and the *S. sanguinis vicR* genes. However, the potential limitation is that the cariogenic biofilm may be more complex, and additional species should be considered to provide cariogenicity ability. Future research is needed to investigate a prolonged observation time for rat caries with or without high sucrose conditions.

In our recently published work,[17] we constructed the aminated dendritic mesoporous silica nanoparticles (DMSNs-NH_2) carrying plasmid-AS*vicR*. The plasmid-AS*vicR* loaded on DMSNs-NH2 could be transformed into *S. mutans*, which reduced EPS synthesis and biofilm organization and showed preliminary anti-caries potential. However, the use of DMSNs-NH_2 is different from that of the materials in the present study. Firstly, the properties of materials are improved and enhanced, in which DMSNs-NH_2 were non-degradable while the SSN is made from natural corn starch and spermine with degradability. The SSN is more biofriendly as a gene carrier. Secondly, the potential applications of the DMSNs-NH_2 and SSN nanoparticles are different. The DMSNs-NH_2 has silicon dioxide as the carrier with a certain hardness and non-degradable properties, and can be used for filling resin or toothpaste filler. The main use of the SSN nanoparticles is developed for mouthwash. Regarding the chemical synthesis process, DMSNs-NH_2 is based on the silicon dioxide while SSN nanoparticles are based on spermine. From this point of view, the SSN nanoparticles in the present article are more innovative and more promising for caries-prevention transformation applications.

5. Conclusions

A SSN material was developed by grafting spermine onto the starch molecule *via* CDI activation. The positively charged SSN exhibited an excellent ability to bind with nucleic acids and protect them from degradation by nucleases. When applied to the oral cavity, the SSN achieved high transformation efficiency in delivering the AS*vicR* plasmid to *S. mutans*. *Via* the targeted posttranscriptional regulation of the *vicR* gene, the SSN-AS*vicR* complex inhibited EPS synthesis and cariogenicity in *S. mutans* without disrupting oral microbiota homeostasis (Scheme 1). Thus, this SSN-AS*vicR* system could be prepared as a ready-to-use formulation targeting cariogenic bacteria, showing great

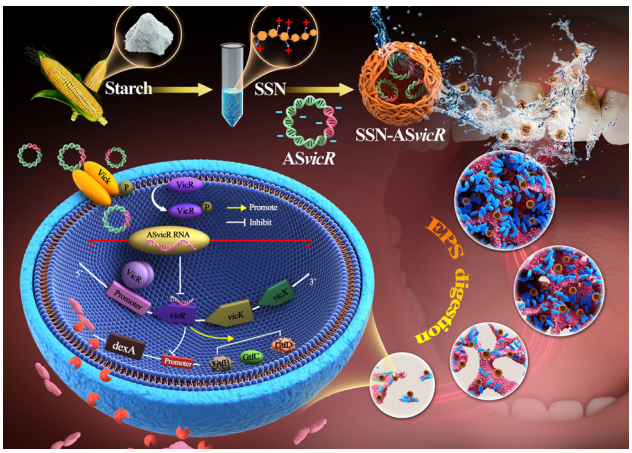

Scheme 1 The molecular schematic diagram of the SSN-AS*vicR* nanoparticles acting on *S. mutans*.

potential in the prevention of dental caries. More importantly, taking into consideration the global antibiotic abuse and multiple drug resistance issues, this SSN material design strategy provides a novel approach for anti-infective treatments based on gene transformation and targeted RNAi.

Data availability statement

The data that support the findings of this study are available from the corresponding author upon a reasonable request.

Author contributions

Lei, L: contributed to conception and design, acquisition and analysis, and drafted and critically revised the manuscript. Zhang, Y: contributed to conception and design, acquisition and analysis, and drafted and critically revised the manuscript. Xu, Y: contributed to conception and design, acquisition and interpretation, drafted the manuscript, and critically revised the manuscript. Tian, Y: contributed to conception and analysis, and critically revised the manuscript. Zhao, J: contributed to conception and analysis, and critically revised the manuscript. Xiang, Y: contributed to conception and analysis, and critically revised the manuscript. Yang, H: contributed to conception and analysis, and critically revised the manuscript. Yang, Y: contributed to conception and design, analysis and interpretation, drafted the manuscript, and critically revised the manuscript. Hu, T: contributed to conception and design, analysis and interpretation, drafted the manuscript, and critically revised the manuscript. All authors gave their final approval and agreed to be accountable for all aspects of the work.

Conflicts of interest

The authors declare no conflicts of interest.

Acknowledgements

This work was supported by the National Natural Science Foundation of China (no. 82170948, 31971196 and 32201096), the Sichuan Science and Technology Program (Grant no. 2021YFS0085 and 2023NSFSC0557), the Research and Development Program of West China Hospital of Stomatology Sichuan University (Grant no. RD-03-202002, RD-03-202103 and RD-02-202001), and the Research Funding from West China School/Hospital of Stomatology Sichuan University (Grant no. RCDWJS2021-13, RCDWJS2020-24 and RD-02-202114).

References

1 GBD 2016 Disease and Injury Incidence and Prevalence Collaborators, *Lancet*, 2017, **390**, 1211–1259.
2 W. H. Bowen and H. Koo, *Caries Res.*, 2011, **45**, 69–86.
3 M. D. Senadheera, A. W. C. Lee, D. C. I. Hung, G. A. Spatafora, S. D. Goodman and D. G. Cvitkovitch, *J. Bacteriol.*, 2007, **189**, 1451–1458.
4 R. N. Stipp, H. Boisvert, D. J. Smith, J. F. Höfling, M. J. Duncan and R. O. Mattos-Graner, *PLoS One*, 2013, **8**, e58271.
5 M. D. Senadheera, B. Guggenheim, G. A. Spatafora, Y.-C. C. Huang, J. Choi, D. C. I. Hung, J. S. Treglown, S. D. Goodman, R. P. Ellen and D. G. Cvitkovitch, *J. Bacteriol.*, 2005, **187**, 4064–4076.
6 L. Lei, R. N. Stipp, T. Chen, S. Z. Wu, T. Hu and M. J. Duncan, *J. Dent. Res.*, 2018, **97**, 1477–1484.
7 L. Lei, B. Zhang, M. Mao, H. Chen, S. Wu, Y. Deng, Y. Yang, H. Zhou and T. Hu, *J. Dent. Res.*, 2020, **99**, 204–213.
8 S. E. Cross, J. Kreth, L. Zhu, R. Sullivan, W. Shi, F. Qi and J. K. Gimzewski, *Microbiology (Reading)*, 2007, **153**, 3124–3132.
9 M. F. Hayacibara, H. Koo, A. M. Vacca-Smith, L. K. Kopec, K. Scott-Anne, J. A. Cury and W. H. Bowen, *Carbohydr. Res.*, 2004, **339**, 2127–2137.
10 H. Shen, X. Huang, J. Min, S. Le, Q. Wang, X. Wang, A. A. Dogan, X. Liu, P. Zhang, M. S. Draz and J. Xiao, *Curr. Top. Med. Chem.*, 2019, **19**, 2507–2523.
11 S. Y. Neshat, S. Y. Tzeng and J. J. Green, *Curr. Opin. Biotechnol*, 2020, **66**, 1–10.
12 A. Ghosal, A. Vitali, J. E. M. Stach and P. E. Nielsen, *ACS Chem. Biol.*, 2013, **8**, 360–367.
13 A. B. Castro-Ceseña, T. A. Camacho-Villegas, P. H. Lugo-Fabres, E. E. Novitskaya, J. McKittrick and A. Licea-Navarro, *Carbohydr. Polym.*, 2016, **148**, 78–85.
14 S. Y. Cheuk, F. F. Shih, E. T. Champagne, K. W. Daigle, J. A. Patindol, C. P. Mattison and S. M. Boue, *Food Chem.*, 2015, **174**, 585–590.
15 M. J. Majcher, A. Babar, A. Lofts, A. Leung, X. Li, F. Abu-Hijleh, N. M. B. Smeets, R. K. Mishra and T. Hoare, *J Controlled Release*, 2021, **330**, 738–752.
16 X. Huang, X. Li, L. Chen and L. Li, *Carbohydr. Polym.*, 2017, **173**, 690–700.

17 Y. Tian, Y. Zhang, M. Zhang, X. Chen, L. Lei and T. Hu, *Int. J. Nanomedicine*, 2022, **17**, 1255–1272.
18 S. A. Engelberth, N. Hempel and M. Bergkvist, *Bioconjug. Chem.*, 2015, **26**, 1766–1774.
19 Y. Jiao, S. Ma, Y. Wang, J. Li, L. Shan, J. Sun and J. Chen, *Int. J. Biol. Sci.*, 2016, **12**, 580–593.
20 Y. Jiao, L.-N. Niu, S. Ma, J. Li, F. R. Tay and J.-H. Chen, *Prog. Polym. Sci.*, 2017, **71**, 53–90.
21 F. Madeo, T. Eisenberg, F. Pietrocola and G. Kroemer, *Science*, 2018, **359**, eaan2788.
22 Y. Liang, C. Piao, C. B. Beuschel, D. Toppe, L. Kollipara, B. Bogdanow, M. Maglione, J. Lützkendorf, J. C. K. See, S. Huang, T. O. F. Conrad, U. Kintscher, F. Madeo, F. Liu, A. Sickmann and S. J. Sigrist, *Cell Rep.*, 2021, **35**, 108941.
23 H. Yang, Y. Yang, B.-Z. Li, B. Adhikari, Y. Wang, H.-L. Huang and D. Chen, *Carbohydr. Polym.*, 2020, **231**, 115692.
24 L. Lei, Y. Yang, M. Mao, H. Li, M. Li, Y. Yang, J. Yin and T. Hu, *Front. Microbiol.*, 2015, **6**, 1432.
25 F. C. Petersen and A. A. Scheie, *Methods Mol. Biol.*, 2010, **666**, 167–180.
26 Z. Xie, T. Okinaga, F. Qi, Z. Zhang and J. Merritt, *Appl. Environ. Microbiol.*, 2011, **77**, 8025–8033.
27 F. Vromman, M. Laverrière, S. Perrinet, A. Dufour and A. Subtil, *PLoS One*, 2014, **9**, e99197.
28 Y. Deng, Y. Yang, B. Zhang, H. Chen, Y. Lu, S. Ren, L. Lei and T. Hu, *Int. J. Oral. Sci.*, 2021, **13**, 45.
29 Y. Xu, A. B. Xepapadeas, B. Koos, J. Geis-Gerstorfer, P. Li and S. Spintzyk, *Dent. Mater.*, 2021, **37**, e314–e327.
30 W. H. Bowen, K. M. Madison and S. K. Pearson, *J. Dent. Res.*, 1988, **67**, 1316–1318.
31 M.-Y. Mao, Y.-M. Yang, K.-Z. Li, L. Lei, M. Li, Y. Yang, X. Tao, J.-X. Yin, R. Zhang, X.-R. Ma and T. Hu, *Front. Microbiol.*, 2016, **7**, 00687.
32 H. Koo, P. L. Rosalen, J. A. Cury, Y. K. Park, M. Ikegaki and A. Sattler, *Caries Res.*, 1999, **33**, 393–400.
33 L. Su, F. Yu, Z. Li, C. Zeng, Q. Xu and M. Fan, *Acta Pharmacol. Sin.*, 2014, **35**, 592–598.
34 Y. Ji, X. Yang, Z. Ji, L. Zhu, N. Ma, D. Chen, X. Jia, J. Tang and Y. Cao, *ACS Omega*, 2020, **5**, 8572–8578.
35 H. Li, B. Zhang, S. Lü, H. Ma and M. Liu, *Int. J. Biol. Macromol.*, 2018, **120**, 1225–1231.
36 Y. Huang, H. Hu, R.-Q. Li, B. Yu and F.-J. Xu, *ACS Appl. Mater. Interfaces*, 2016, **8**, 3919–3927.
37 Y. Chu, Y. Sun, W. Wu and H. Xiao, *Carbohydr. Polym.*, 2020, **250**, 116892.
38 T. Eisenberg, H. Knauer, A. Schauer, S. Büttner, C. Ruckenstuhl, D. Carmona-Gutierrez, J. Ring, S. Schroeder, C. Magnes, L. Antonacci, H. Fussi, L. Deszcz, R. Hartl, E. Schraml, A. Criollo, E. Megalou, D. Weiskopf, P. Laun, G. Heeren, M. Breitenbach, B. Grubeck-Loebenstein, E. Herker, B. Fahrenkrog, K.-U. Fröhlich, F. Sinner, N. Tavernarakis, N. Minois, G. Kroemer and F. Madeo, *Nat. Cell Biol.*, 2009, **11**, 1305–1314.
39 Y. Jiang, X. Pan, J. Chang, W. Niu, W. Hou, H. Kuai, Z. Zhao, J. Liu, M. Wang and W. Tan, *J. Am. Chem. Soc.*, 2018, **140**, 6780–6784.
40 H. Chan, B. Söderström and U. Skoglund, *MicrobiologyOpen*, 2020, **9**, e999.
41 Z. D. Moye, M. Son, A. E. Rosa-Alberty, L. Zeng, S.-J. Ahn, S. J. Hagen and R. A. Burne, *Appl. Environ. Microbiol.*, 2016, **82**, 4821–4834.
42 Y. Sato, K. Okamoto-Shibayama and T. Azuma, *J. Oral. Microbiol.*, 2013, **5**, 21285.
43 C. L. Simpson and R. R. Russell, *J. Bacteriol.*, 1998, **180**, 4711–4717.
44 M. Kruppa and R. Calderone, *FEMS Yeast Res.*, 2006, **6**, 149–159.
45 A. Gedif Meseret, *Int. J. Oral Dent. Health*, 2021, **7**, 127.
46 H. Wu, Y. Ma, X. Peng, W. Qiu, L. Kong, B. Ren, M. Li, G. Cheng, X. Zhou and L. Cheng, *Arch. Oral Biol.*, 2020, **114**, 104730.
47 F. Manji, G. Dahlen and O. Fejerskov, *Caries Res.*, 2018, **52**, 548–564.
48 N. Philip, B. Suneja and L. J. Walsh, *Caries Res.*, 2018, **52**, 153–165.
49 W. Li, E. S. Thian, M. Wang, Z. Wang and L. Ren, *Adv. Sci.*, 2021, **8**, e2100368.
50 Y. Yang, M. Mao, L. Lei, M. Li, J. Yin, X. Ma, X. Tao, Y. Yang and T. Hu, *Mol. Oral Microbiol.*, 2019, **34**, 51–63.
51 Y. Hu, A. Amir, X. Huang, Y. Li, S. Huang, E. Wolfe, S. Weiss, R. Knight and Z. Z. Xu, *Genome Res.*, 2022, **32**, 1112–1123.

